Available online at www.sciencedirect.com

ScienceDirect

journal homepage: http://www.elsevier.com/locate/acme

Original Research Article

Experimental and numerical investigation of lead-rubber dampers in chevron concentrically braced frames

Keyvan Zeynali [a], *Habib Saeed Monir* [a], *Nadia M. Mirzai* [b], *Jong Wan Hu* [c,d,*]

[a] *Department of Civil Engineering, Urmia University, Urmia, Iran*
[b] *School of Civil Engineering, University of Tehran, Tehran, Iran*
[c] *Department of Civil and Environmental Engineering, Incheon National University, 12-1 Songdo-dong, Yeonsu-gu, Incheon 22012, South Korea*
[d] *Head of Center, Incheon Disaster Prevention Research Center, Incheon National University, 12-1 Songdo-dong, Yeonsu-gu, Incheon 406-840, South Korea*

ARTICLE INFO

Article history:
Received 6 January 2017
Accepted 18 June 2017
Available online 14 July 2017

Keywords:
Lead-rubber bearing
Shaking table tests
Hyper-elastic
Finite element analysis

ABSTRACT

This paper presents a theoretical and experimental evaluation of the application of lead rubber dampers (LRD) in the chevron bracing of structures. This device consists of a circular lead core with several layers of steel and rubber plates that are sandwiched together. This damper was manufactured at the earthquake engineering laboratory of Urmia University and installed inside a SDOF steel frame. The frame was placed on a shaking table, and its responses under several earthquake excitations were recorded. A 3D finite element model was created for the device, and hyper-elastic properties were determined for the rubber layers. To check the effectiveness of the device in mitigating the responses of multi-story frames, several nonlinear time history analyses were conducted on the structures using three earthquake excitations. The results indicate that significant reductions in the stories' drift can be achieved by installing lead-rubber dampers in the chevron bracing.

1. Introduction

The majority of buildings undergo dynamic loading, which may originate from wind loads, seismic excitation or various other sources. In several instances, particularly upon being subjected to strong earthquakes, vibrations can lead to structural damage or even collapse. The higher the intrinsic or natural damping in the structures is, the lower the probability is that damage will occur. For frames under strong seismic loads, the intrinsic damping is not sufficient to alleviate structural responses, in which case additional damping can be employed. The supplemental damping can be classified into three groups: passive control

* *Corresponding author at*: Department of Civil and Environmental Engineering, Incheon National University, 12-1 Songdo-dong, Yeonsu-gu, Incheon 22012, South Korea.
E-mail addresses: k.e.zeynali@gmail.com (K. Zeynali), h.s.monir@mail.urmia.ac.ir (H. Saeed Monir), nmirzai@ut.ac.ir, nadia.m.mirzai@gmail.com (N.M. Mirzai), jongp24@inu.ac.kr (J.W. Hu).
http://dx.doi.org/10.1016/j.acme.2017.06.004

systems, active and semi-active systems, and base isolators [1–3].

The joints of these systems all require power to produce forces to control the structural responses. However, the power source is distinct in each system. In passive systems, the controlling forces are generated at the points of attachment to the structure, and the power required to extend such forces originates from the motion of these points. The direction and amplitude of these forces are specified by the relative motion of the points. In active systems, a controller is annexed to the structure to develop the motion control forces. The direction and magnitude of these forces are specified based on the controller input data, which are obtained through a wide range of sensors. Several features of semi-active systems are similar to those of passive devices, but semi-active systems use battery power controllers to regulate the mechanical properties of the dampers. The forces in both purely passive and semi-active devices expand from the motion of sticking points [4–6].

Base isolation is another system used for structural control. Seismic isolation is other design mechanism that suggests decoupling a structure or a portion of it from the damaging effects of ground accelerations [7,8]. The Foothill Communities Law and Justice (FCLJC) in 1984 was the first structure in the United States with high damping rubber bearings [9]. The Emergency Operations Center (EOC) in Los Angeles County employed 28 high-damping rubber bearings [10]. Nonlinear time history analyses of isolated systems have usually been carried out by using bounding analysis to determine the response of the isolated structures. Performing a bounding analysis accounts for the history of the loading and heating effects [11]. However, most of the differences between the upper and lower bound properties emerge due to heating effects [12]. Passive control dampers can be classified into two groups: permanent and disposable devices (although adjustments might be required after dissipation) [13]. This paper presents the results of an experimental and theoretical evaluation of the application of lead-rubber dampers in the chevron bracing of structures. This device is a passive control system and requires no external power to dissipate seismic energy. In this proposed damper, yielding of the lead plug is the energy dissipating phenomenon. The lead-rubber damper falls in the permanent systems category.

2. Structural system components

2.1. *Rubber layers*

Rubber has numerous properties that make it beneficial in a difference of engineering applications, such as in tire technology, structure foundations, dampers and base isolators. Rubber can deform elastically with large deformations and then return to its initial shape after loading. Rubber has been used extensively in structures for seismic protection, such as viscoelastic dampers or base isolation systems [14].

In the current proposed lead-rubber isolation system, rubber is used between the steel layers to allow them to slip over each other and resist lateral loading.

2.2. *Lead core*

The purpose of concatenating a lead core into steel-rubber layers is to attach an elastic perfectly plastic element to the hysteresis loop of the device. The lead core will have a certain yield level, which is a function of the theoretical yield limit of lead (10.5 MPa) and the degree of its confinement [10]. As the confinement of the lead core increases, the hysteresis loop of the core will move more toward an elastic-plastic system.

Confinement of the lead core is provided by the following three mechanisms:

1. Internal shims hold the lead from the structure into the rubber layers.
2. Restricting plates are used at the top and bottom of the lead core.
3. A vertical compressive load is applied on the lead core.

The successful operation of the device depends on the quality of the lead, which recovers and re-crystallizes rapidly. For long-term forces, lead will creep, and the maximum force in the core will be less than the yield force subjected to applied forces. For structures such as bridges, where non-seismic displacements are applied to the bearings, this property will change the maximum transmitted force because of creep, shrinkage and temperature influences.

3. Mechanical characteristics of lead-rubber damper

Lead rubber dampers consists of a circular lead core and several alternating layers of rubber and steel plates. The rubber layers are sandwiched between steel layers. The device is shown in Fig. 1.

The steel layers move over each other through the exertion of the external loading. The lead core resists the displacement of the steel layers and undergoes plastic deformations, which result in the dissipation of seismic forces by the system.

The lead-rubber damper has a nonlinear load displacement relation, similar to the lead-rubber isolators. This one, termed a hysteresis loop, describes the effective stiffness and hysteresis damping provided by the system. Fig. 2 shows a typical hysteresis loop for the lead-rubber damper.

Lead-plug bearings are always simulated as bilinear elements with properties based on the three parameters K_1, K_2, and Q, as shown in Fig. 2. The elastic stiffness K_1 is not easy to measure and is generally taken as an empirical multiple of K_2, the post-yield stiffness, which can be measured from the shear modulus of the rubber and the bearing design. The feature strength Q is the intercept of the hysteresis loop along the force axis and is exactly measured from the yield stress of the lead and lead-plug area [10].

In terms of the basic parameters K_1, K_2, and Q, the effective stiffness of the lead-plug bearing is given by Eq. (1).

$$K_{eff} = K_2 + \frac{Q}{D} \quad D \geq D_y \tag{1}$$

where D_y is the yield displacement.

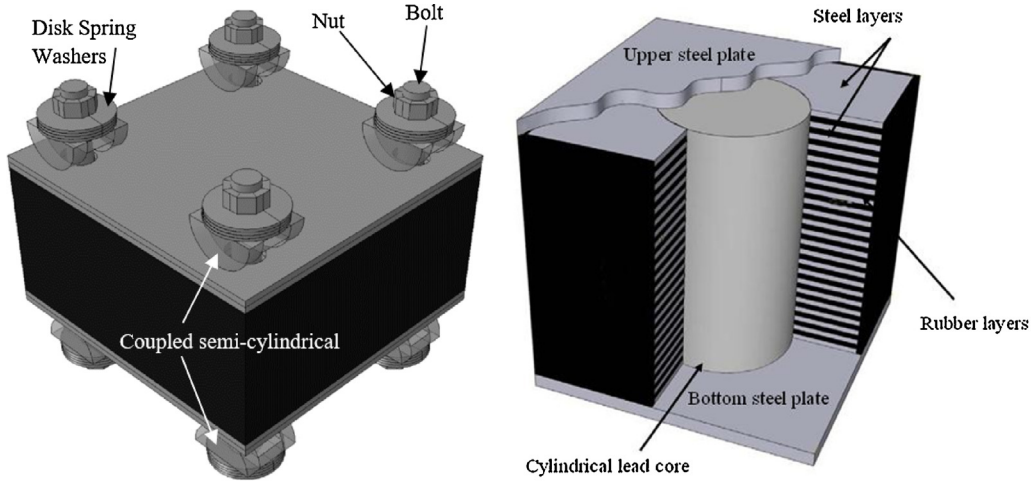

Fig. 1 – Schematic figure of the lead-rubber damper.

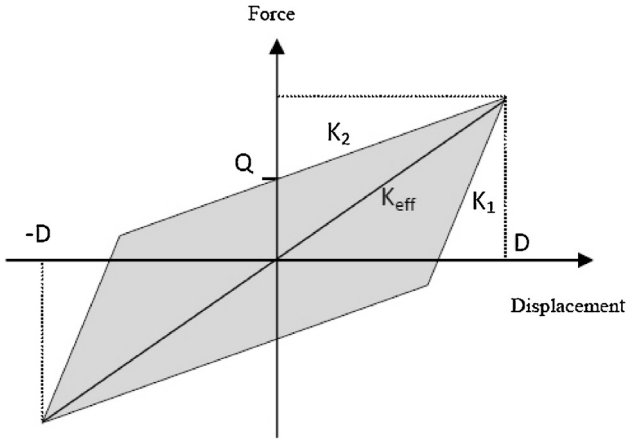

Fig. 2 – Schematic hysteresis loop of lead-rubber damper.

The effective damping β_{eff} for $D \geq D_y$ is defined as:

$$\beta_{eff} = \frac{A}{2\pi K_{eff} D^2} \tag{2}$$

where A is the area of hysteresis loop. There are various parameters that can be manipulated to control the behavior of the system. These variables are:

- The dimension (*l*) and thickness (*t*) of the steel and rubber layers and the diameter (*d*) and height (*h*) of the lead core.
- The length (*l*), thickness (*H*) and width (*b*) of the device.
- The hysteresis behavior and mechanical properties of the lead core.

The $Sn_{63}Pb_{37}$ lead/tin alloy was tested under compressive loading by Jenq et al. [15]. Kalpakidis and Constantinou [12] presented experimental results of the tensile tests on lead specimen under various strain rates and temperatures. In the device, the $Sn_{63}Pb_{37}$ alloy was used for the lead plug. The properties of the alloy at room temperature are available in the works above. The 63% tin 37% lead solder alloy leads to the maximum of the tensile strength, shear and impact strength, and creep strength. The tin-lead alloy has a lower melting point and higher tensile strength than pure lead. Once the tin/lead alloy becomes semi-solid due to vibrations, it solidifies immediately after the elimination of the excitation without the pasty phase such as other alloys. This permits soldering and fast cyclic times. Therefore, after the excitations, the lead plug in the damper solidifies, and the structure remains stable.

4. Finite element analysis

Finite element analysis was conducted to determine the behavior of the system. Hyper-elastic properties were considered for the rubber layers, and the plastic behavior of the lead core was simulated using the Von Misses yield criterion. The lead rubber bearing was modeled using ABAQUS based on [16]. Eight-node linear brick, three dimensional hexahedral, reduced integration, and hourglass control solid elements were used to model the components. This element has three translations and three rotational degrees of freedoms at each node. Solid elements of 2 mm and 5 mm size in length were used to mesh the lead core model and the other parts of model respectively. The finite element model of the system is shown in Fig. 3.

To define the hyper-elastic behavior of the rubber layers, the stored strain energy function *U* was incorporated, which defines the stored strain energy in a material per unit volume.

The stress–strain relationship of a hyper-elastic material can be calculated using Eq. (3).

$$\sigma_{ij} = \frac{\partial U(\epsilon)}{\partial \epsilon_{ij}} \tag{3}$$

where σ_{ij} and ϵ_{ij} represent the stress and strain components, respectively.

Various models can be employed to simulate the hyper-elasticity, such as Van der Waals, Arrude-Boyce, Neo-Hookean, Mooney-Rivlin, Ogden, Reduced polynomial, Polynomial, and Yeoh models [17–20]. Most of these models are composed of polynomial equations.

Raos [21] investigated the feasibility of estimating the test results using the Van der Waals, Mooney-Rivlin, Neo-Hookean and Ogden models. The test results were captured from the

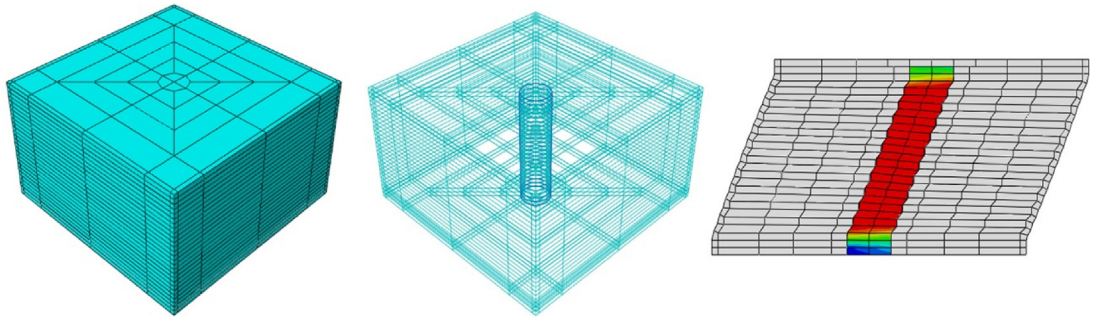

Fig. 3 – Finite element model of the device.

conducted uniaxial and biaxial tensile and compressive tests on the SBR rubber vulcanizate. These experimental tests covered a vast range of deformations (extension ratio λ from 0.5 to 4.0). Based on the results of this investigation, it was concluded that the Neo-Hookean and Mooney-Rivlin models can estimate the test results in compression and moderate tension only at extension ratios λ less than 1.8, whereas the Van der Waals and Ogden models can estimate test results with satisfactory approximation for full assumed range.

The Ogden model is described below, and it was used in this work to model the hyper-elastic behavior of the applied viscoelastic material in the device.

The strain energy function of the Ogden model is defined as

$$U = \sum_{i=1}^{w} \frac{2\mu_i}{\alpha_i^2}\left(\overline{\lambda}_1^{\alpha_i} + \overline{\lambda}_2^{\alpha_i} + \overline{\lambda}_3^{\alpha_i} - 3\right) + \sum_{i=1}^{w} \frac{1}{D_i}\left(J^{el} - 1\right)^{2i} \tag{4}$$

where μ_i and α_i are the temperature-dependent material variables that describe the shear behavior of the material and D_i are the temperature-dependent material variables that describe the compressibility and $\overline{\lambda}_i$ is the deviatoric principal stretches that can be calculated from Eq. (5),

$$\overline{\lambda}_i = J^{-1/3}\lambda_i \tag{5}$$

where J is the total volume ratio expressed by Eq. (6),

$$J = \frac{\lambda_1\lambda_2\lambda_3}{V_0} \tag{6}$$

where V_0 is the original volume of the rubber block and J^{el} is the elastic volume ratio given by Eq. (7).

$$J^{el} = \frac{J}{J^{th}} \tag{7}$$

in which Jth is the thermal volume ratio calculated from Eq. (8).

$$J^{th} = \left(1 + \epsilon^{th}\right)^3 \tag{8}$$

where ϵ^{th} is the linear thermal expansion strain. To model the incompressibility and isothermal response of the assumed materials, the second term in the strain energy function was set to zero. Therefore, the strain function for the Ogden model was obtained from Eq. (9).

$$U = \sum_{i=1}^{w} \frac{2\mu_i}{\alpha_i^2}\left(\overline{\lambda}_1^{\alpha_i} + \overline{\lambda}_2^{\alpha_i} + \overline{\lambda}_3^{\alpha_i} - 3\right) \tag{9}$$

Uniaxial and biaxial tension-compression test results are essential to model the hyper-elastic behavior of rubber. Yoshida et al. [22] presented the test results of uniaxial and biaxial conducted tensile experiments on high damping rubber (HDR-A). However, the results of compressive tests on the high-damping rubber samples are required to better model the hyper-elastic behavior of the rubber block. Amin et al. [23] showed the results of uniaxial compressive tests on high damping rubber. The experimental results, which have been employed in this paper to model the hyper-elastic behavior of rubber blocks, is shown in Fig. 4 [22,23].

To model the plasticity, the true stress and true strain should be used instead of the nominal stress and strain. The true strain, ε, can be obtained from Eq. (10).

$$\epsilon = \ln(1 + \epsilon_{nom}) \tag{10}$$

where ε_{nom} is the nominal strain. The relationship between the true stress and nominal stress is defined as

$$\sigma = \sigma_{nom}(1 + \epsilon_{nom}) \tag{11}$$

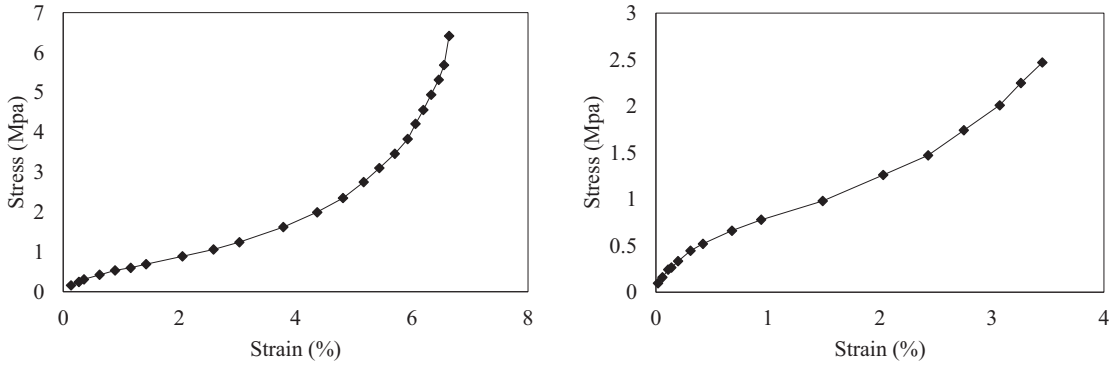

Fig. 4 – Results of the conducted experimental tests on rubber from the literature [22,23].

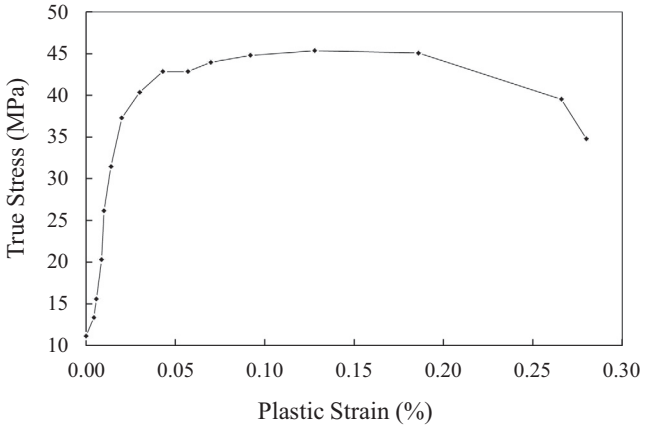

Fig. 5 – True stress–plastic strain curve of lead.

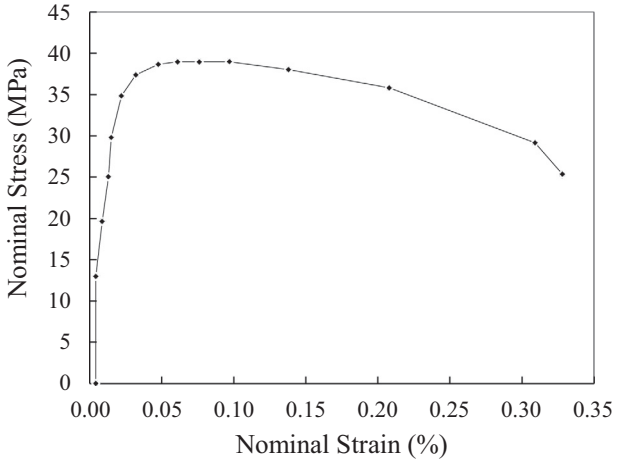

Fig. 6 – Engineering stress–strain curve of lead [18].

The calculated true strain from the above equations is a composition of the elastic and plastic strain. Accordingly, the plastic strain may be calculated from Eq. (12).

$$\epsilon_{pl} = \epsilon_t - \epsilon_{el} = \epsilon_t - \frac{\sigma}{E} \tag{12}$$

in which ε_{pl} is the true plastic strain, ε_t is the true total strain, σ is the true stress and E is the modulus of Yang [17].

To obtain the stress–strain properties of the lead core, a series of experiments have been previously conducted on several specimens [24]. The true strain curve, which was considered for the lead core in this work, is shown in Fig. 5. The applied engineering stress–plastic strain curve to obtain the true stress–plastic strain curve is shown in Fig. 6.

An isotropic hardening model was employed to model the hardening effect of the lead core. This model assumes that the center of the yield surface remains unchanged in the stress space. However, the size of yield surface varies uniformly in all directions from the yield stress that changes based on the plastic strains. This model is generally used for metal plasticity and is helpful in problems involving gross plastic straining [17–20]. The Newton's method is used to solve nonlinear equations of LRD model in ABAQUS. Also, the Newmark method is employed to solve the equation of motion in the direct integration time history analysis in the finite element models that conducted by SAP2000.

5. Shaking table and the superstructure

The shaking table of Urmia University has one degree of freedom which consists of a deck, an actuator which applies the excitation and a computer unit which controls the actuator, and the details of its superstructure are shown in Fig. 7. It is a three dimensional frame which has been installed over the shaking table. In one direction, the excitations are applied and along the other direction, the frame is braced. The weight of the roof is 115 kg but four point loads can be also applied at the corners by using steel sinkers. The entire mass of the roof was 443 kg. The base excitations are applied by using horizontal computer-controlled actuator. The actuator can produce a stroke of ±125 mm and its velocity is 300 millimeter per second with 1.5 g maximum acceleration. The horizontal acceleration was measured by accelerometers at the bottom and top of the frame. The relative displacement between the bottom and top of the superstructure and shaking table was measured using a *LVDT*. The dynamic behavior of the superstructure was recorded with a digital data logger, and Fig. 8 shows the shaking table unit. To avoid out of plane movements of the frame, it is laterally braced by four steel sticks at the back and the front faces (Figs. 7 and 8).

6. Designing of the lead-rubber damper

Considering the number and dimensions of the rubber and steel layers and the sizes of the lead core, a trial and error method was considered to obtain the required seismic performance. Several finite element models of the damper, whose configurations are shown in Table 1, were created first

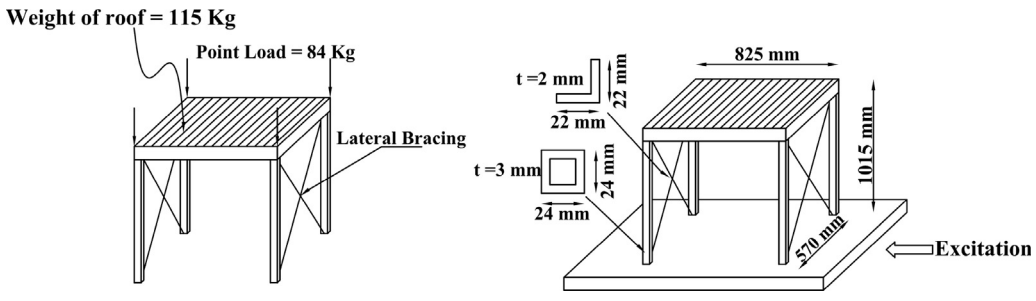

Fig. 7 – Details of the SDOF superstructure.

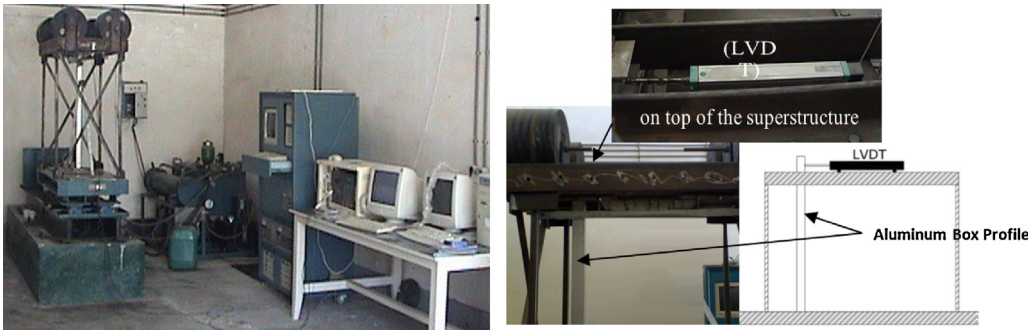

Fig. 8 – Shaking table unit.

Table 1 – Configuration of the models.

Model	t_S (m)	t_R (m)	n_S	n_R	D_L (m)	N_E	N_N
M1	0.002	0.002	12	11	0.014	1544	2378
M2	0.002	0.002	12	11	0.03	1544	2378
M3	0.002	0.002	23	22	0.03	2000	2856
M4	0.002	0.002	12	11	0.04	1544	2378
M5	0.002	0.002	23	22	0.04	2000	2856
M6	0.002	0.002	12	11	0.05	1544	2378

Table 2 – Ground motion records for the SDOF analysis and experimental study.

Earthquake	Station	Magnitude	Latitude	Longitude
Tabas (1978-09-16)	Iran, 9101 Tabas	7.35	33.5800	56.9200
Imperial Valley (1940-5-19)	Array #9, El Centro	6.95	32.7940	−115.549
Kobe, Japan (1995-01-16)	99999 TOT	6.90	35.4850	134.2400

(where t_S is the thickness of the steel plates, t_R is the thickness of the rubber plates, n_S and n_R are the number of steel and rubber layers, respectively, D_L is the diameter of the lead core, N_E is the number of elements and N_N is the number of nodes in finite element model). Then, these models were analyzed under a zigzag top displacement loading, as shown in Fig. 9, to determine their load-deflection curves. The results are shown in Fig. 10 for all models. The model of frame was created using each of the dampers in Table 1, and the models were analyzed numerically under several earthquake excitations, as listed in Table 2. The ground motion records were scaled to produce the spectral accelerations of 0.3 g, 0.75 g and 0.9 g based on the fundamental period and assumed damping ratio, as shown in Table 3.

By comparing the results, model M_1 was chosen to be manufactured and installed in the frame. The subsequent experimental tests were conducted on the system.

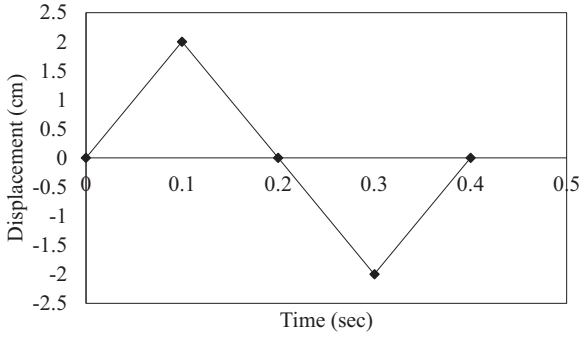

Fig. 9 – Zigzag loading of the damper.

7. Experimental work

The frame without the damper system experienced three earthquake excitations, as listed in Table 2, and its drifts were recorded. Then, the frame was equipped with the lead rubber damper, as shown in Fig. 11, and tested under the same excitations. Fig. 12 shows the location and installation details of the LRD in the SDOF structure, and a detailed description of the device is shown in Fig. 13. The results of the frame in both equipped and unequipped conditions are shown in Figs. 14–16.

It should be noted that in seismic design of structures the displacement value plays an important role, so in this paper, maximum value of displacement has been adopted as a key parameter which may not be occurred at the same time, necessarily.

The effectiveness of these dampers subjected to the scaled El Centro, Kobe and Tabas earthquakes is listed in Table 4. This table shows a comparison of the peak displacement responses of the structure with and without the lead-rubber damper under the three earthquakes. It can be observed that the damper provides significant additional damping to the structure so the displacement of the frame decreases and the structure remains elastic.

8. The comparison of numerical and experimental results

Fig. 17 shows the comparison of numerical and experimental displacements of the frame without the damper under the 0.58 g

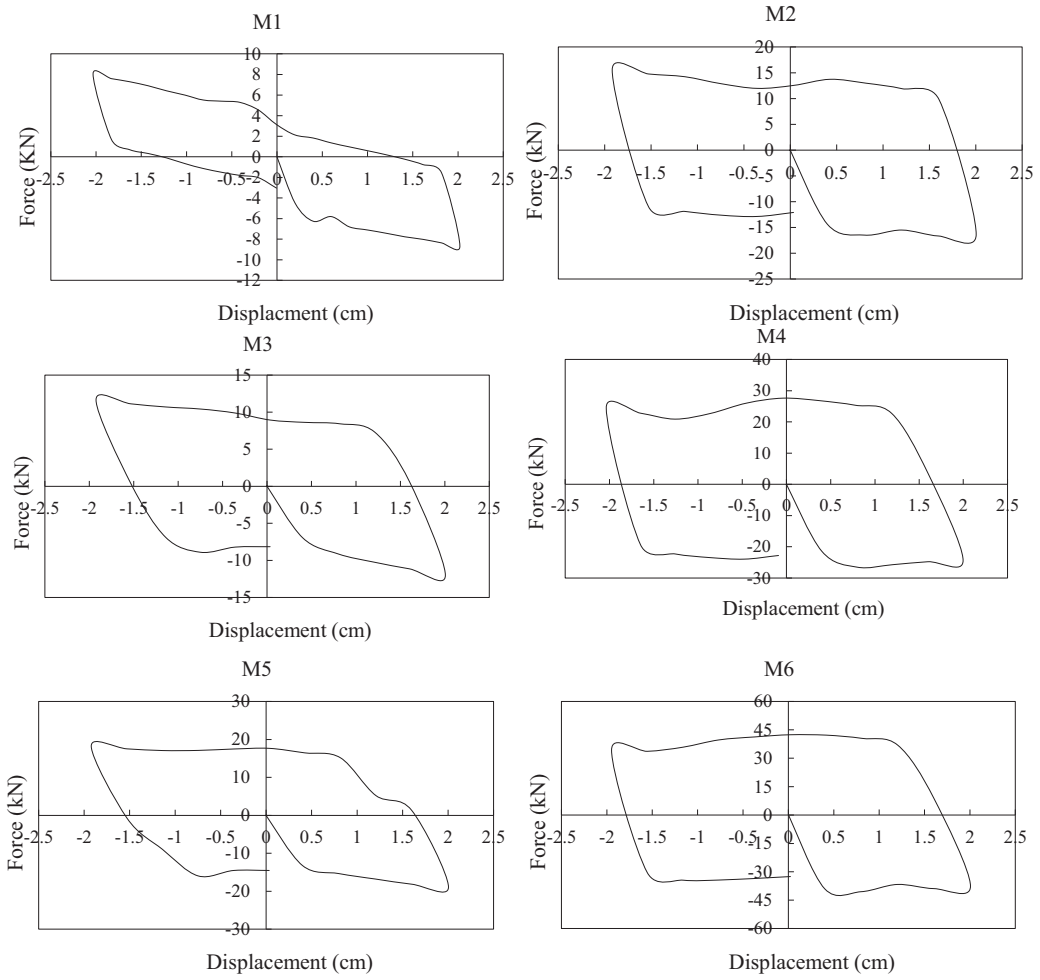

Fig. 10 – Displacement–force curves.

Table 3 – Peak earthquake intensity and the displacement of the structure.

Earthquake	Spectral acceleration (g)	Maximum displacement of the shaking table (mm)						
		W/O damper	With damper					
			M1	M2	M3	M4	M5	M6
Tabas, Iran (1978-09-16)	0.30	10.85	2.26	0.89	1.95	0.59	0.81	0.213
	0.75	27.13	5.384	2.22	5.02	1.47	2.03	0.53
	0.90	32.55	5.77	2.67	5.66	1.76	2.43	0.64
Elcentro, Imperial Valley (1940-5-19)	0.30	10.89	1.43	0.7	1.33	0.43	0.74	0.25
	0.75	27.21	3.58	1.75	3.33	1.08	1.84	0.62
	0.90	32.64	4.41	2.1	4.00	1.29	2.21	0.75
Kobe, Japan (1995-01-16)	0.30	9.62	0.92	0.4	0.8	0.28	0.43	0.164
	0.75	24.04	2.29	0.997	2.00	0.70	1.074	0.41
	0.90	28.84	2.75	1.20	2.40	0.84	1.29	0.492

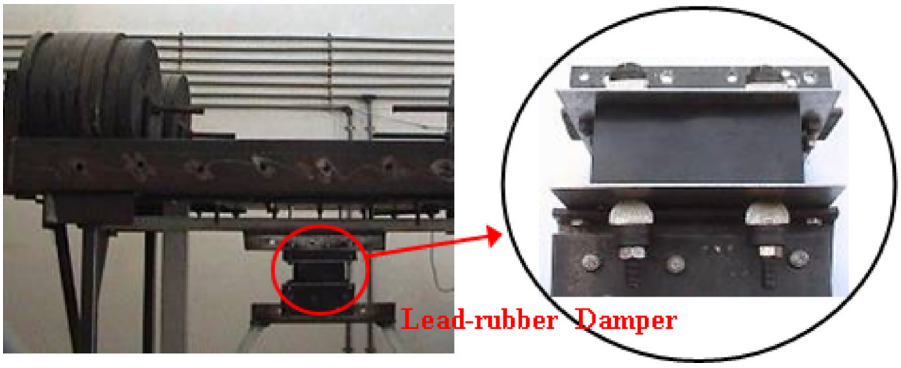

Fig. 11 – Shaking table with the lead-rubber damper.

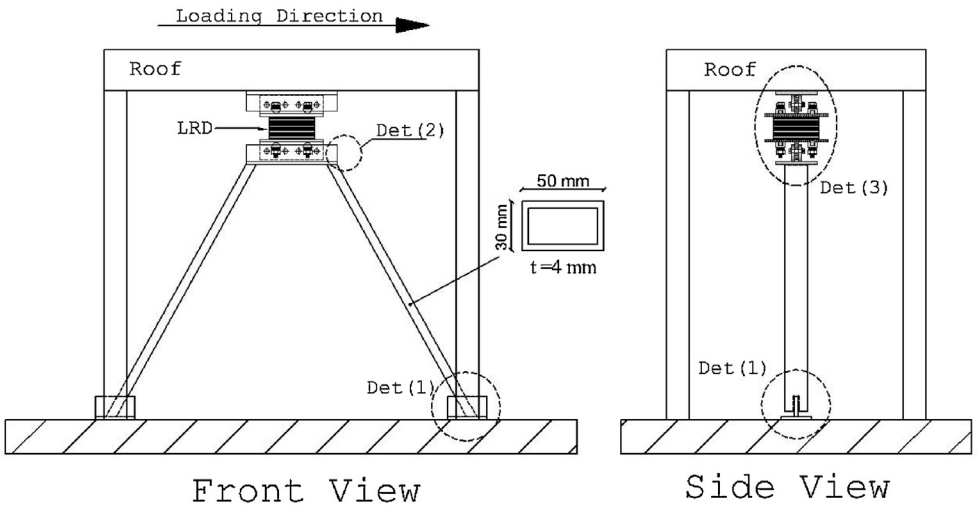

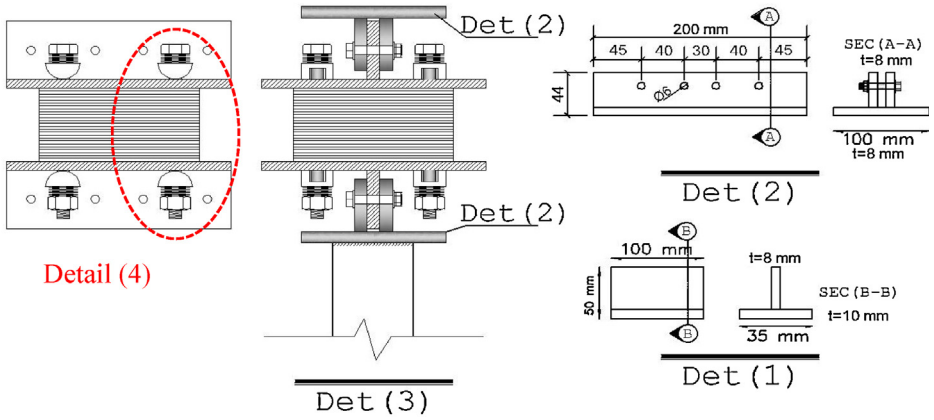

Fig. 12 – Location of the lead-rubber damper in the SDOF frame and details of the installation of the LRD in the frame.

El Centro earthquake. It can be observed that the two curves are in good agreement. Fig. 18 indicates good agreement between the numerical and experimental displacement time histories at the frame with the lead-rubber damper under the 0.7 g El Centro earthquake. The average value of the predicted time–displacement curve was found to be nearly the same as that obtained from the experiment with a maximum variation of 7%. Thus, a reasonably good match was also noticed between the experimentally obtained and predicted curve of time–displacement behavior of the specimen and the model.

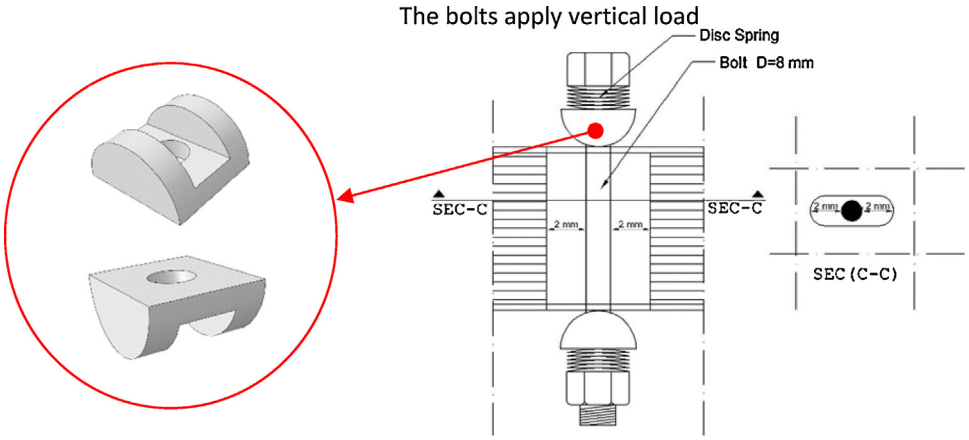

Fig. 13 – Description of the detail (4).

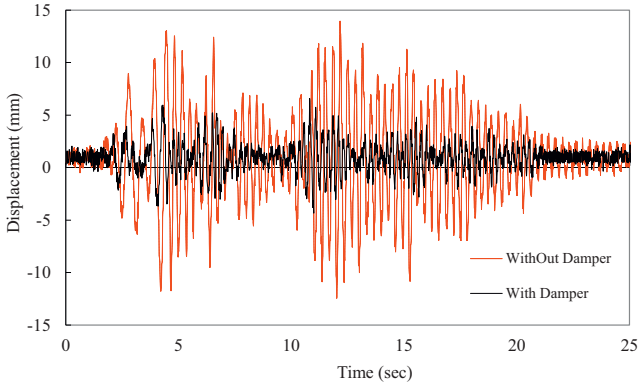

Fig. 14 – Roof displacement histories, Elcentro 0.9 g, with and without the damper.

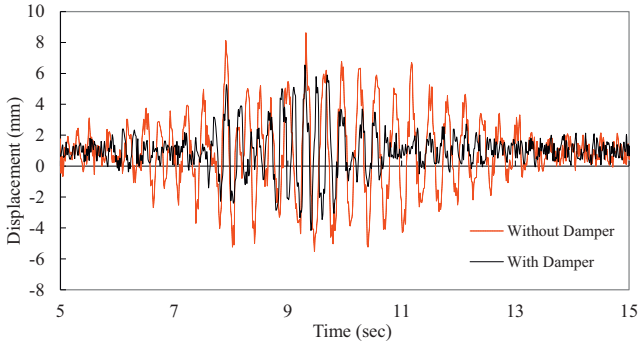

Fig. 15 – Roof displacement histories, Kobe 0.9 g, with and without the damper.

9. Numerical analysis of multi-story structure with a lead-rubber damper

To specify the influence of the LRD on the responses of multi-story structures under seismic excitations, the model of the Lead-rubber damper was inserted in the model of a four-story, three-bay, moment-resisting steel frame. The configuration of this steel frame, equipped with the lead rubber devices, is shown in Fig. 19(b). The typical story height and bay width were 3.20 m and 4 m, respectively. The dead and live gravity loads considered in the design were selected according to the Iranian National Building Code: Part 6. The dead and live loads of the first through 3rd stories were 2.4 Ton/m and 1 Ton/m,

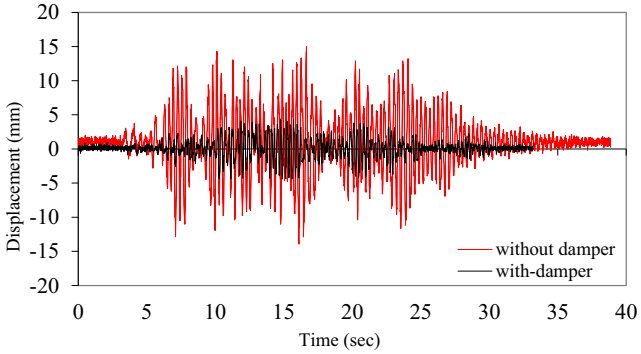

Fig. 16 – Roof displacement histories, Tabas 0.9 g, with and without the damper.

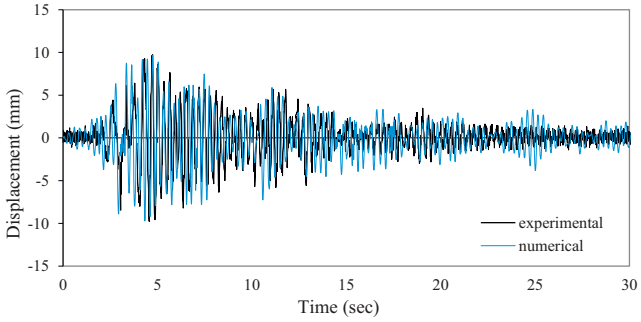

Fig. 17 – The time–displacement curve at the roof of the structure without the damper.

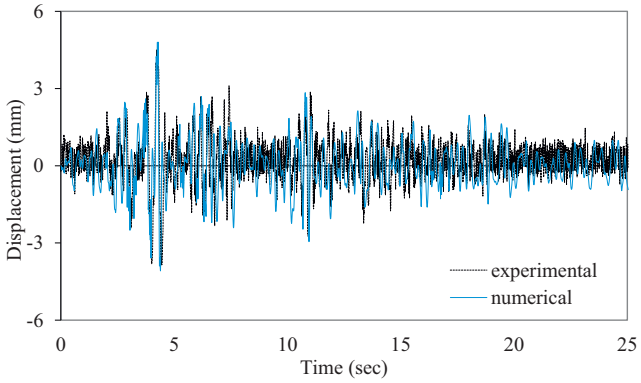

Fig. 18 – Time–displacement curve of the roof of the structure with the lead-rubber damper.

Table 4 – Displacement peaks and reduction rates under several earthquakes.

Earthquake	Peak ground acceleration (g)	Displacement		
		Bare structure (mm)	With damper (mm)	Reduction percentage (%)
Elcentro, Imperial Valley (1940-5-19)	0.77	12.51	6.171	50.67
	0.9	13.95	6.58	52.83
Kobe, Japan (1995-01-16)	0.62	14.87	4.73	68.19
	0.88	16.47	5.6	67
Tabas, Iran (1978-09-16)	0.8	14.32	6.09	57.47
	0.9	14.98	6.29	58.01

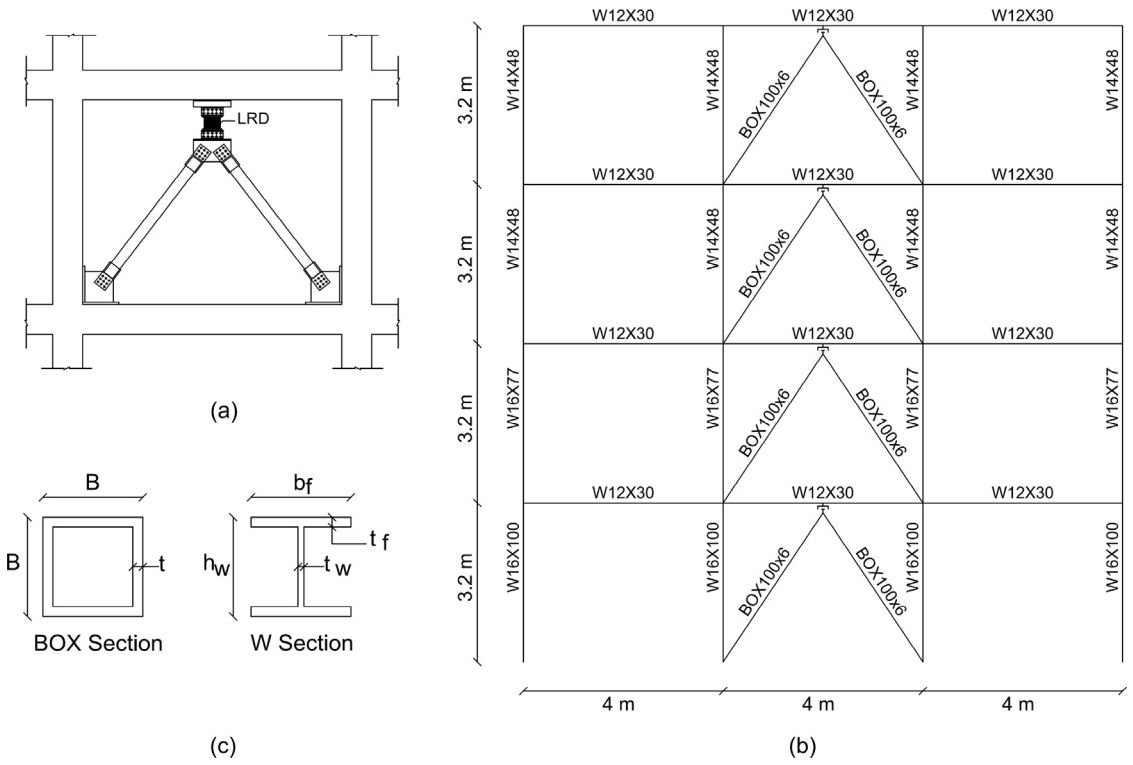

Fig. 19 – (a) Overall location of the LRD on the chevron bracing (b) four-story steel frame with the damper (c) the beam, column and brace cross sections.

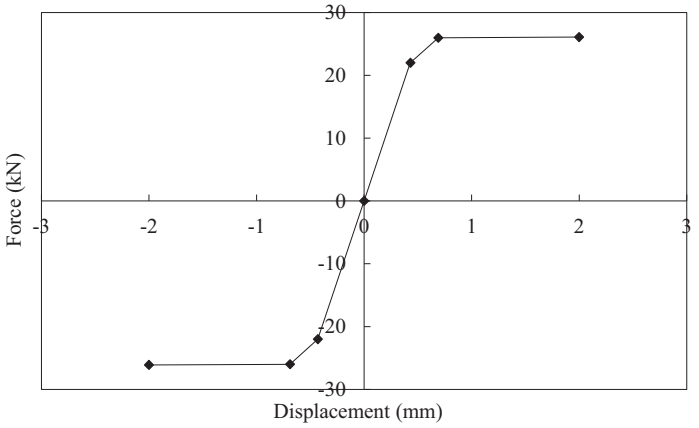

Displacement (cm)	Force (KN)
-2	-26.1
-0.69	-26
-0.43	-22
0	0
0.43	22
0.69	26
2	26.1

Fig. 20 – Link element properties of the LRD-M4 in the 4-story steel frame.

Table 5 – Ground motion records for the nonlinear analysis of the multi-story frame.

Earthquake	Station and direction	Magnitude	Duration(s)
Imperial Valley-02, 1940	El Centro, Array #9-270°	6.95	53.43
Kobe, Japan, 1995	Kobe university-90°	6.90	31.97
Tabas, Iran-1978	Sedeh-L1	7.35	39.94

Table 6 – The frame designed sections.

Section name	hw (mm)	tw (mm)	bf (mm)	tf (mm)
W16×100	431	15	265	25
W16×77	420	12	262	20
W14×48	350	10	204	15
W12×30	314	6	166	12
BOX100×6	B (mm)		t (mm)	
	100		6	

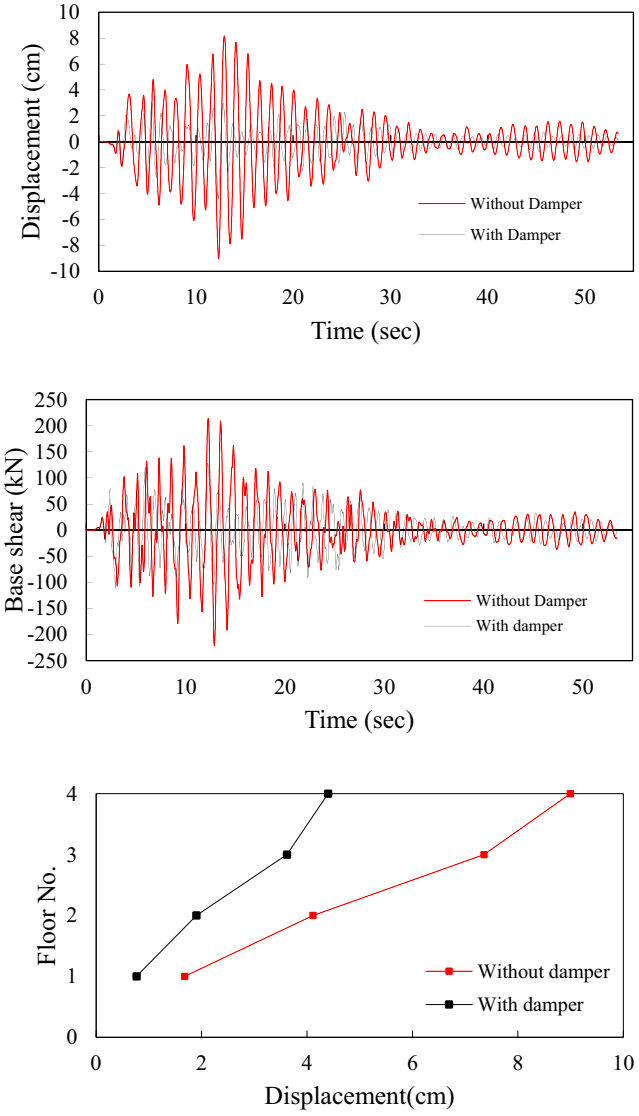

Fig. 21 – Effect of using one LRD per floor on the response of the 4-story steel frame under the Imperial Valley 0.1 g earthquake.

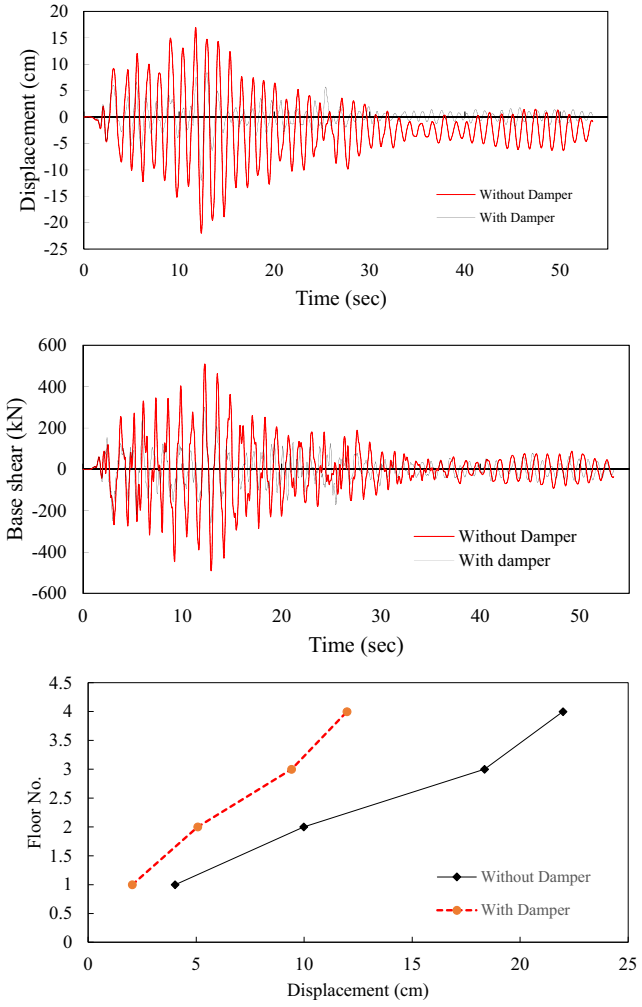

Fig. 22 – Effect of using one LRD per floor on the response of the 4-story steel frame under the Imperial Valley 0.25 g earthquake.

and those for the 4th story were 2.20 Ton/m and 0.6 Ton/m, respectively. The designed sections are shown in Fig. 19(b). The typical frame cross sections are shown in Fig. 19(c). The sections of the frame, shown in Table 6 were made from structural steel ST52 (based on DIN standard) with a 345 MPa yield strength and 500 MPa ultimate strength. To model the nonlinear response of the structure, the SAP2000 software was employed, and the FEMA356 code provided the hinge specifications. The periods of the first and second modes of the structure were 1.168 and 0.426 s, respectively. A 3% damping was assumed for each mode.

This 2D steel frame was analyzed based on the nonlinear time history under the scaled El Centro, Kobe and Tabas earthquake records, including the P-delta plus large displacement effects. A description of these earthquakes is shown in Table 5. Multi linear plastic link elements were used to model the hysteretic behavior of the damper. The model M4 from Table 1 was chosen to be installed in the frame. Fig. 20 shows the link element properties that were used as the LRD.

The response of the steel frame equipped with the devices was compared to that of the unequipped frame, and the results are shown in Figs. 21–30. The proposed device can be installed on top of the chevron brace of a frame, as shown in Fig. 19(a). Actually, under high values of the peak accelerations (for example 0.75 g and 0.9 g) the MDOF model experiences very large demands and the structure collapses. For comparison the efficiency of proposed device during total time of earthquake, the MDOF was subjected to low peak accelerations.

Based on these results, the effectiveness of the LRD in mitigating the structural vibration is clear. The comparison of the roof displacements indicates that the structure with the LRD remains elastic, whereas the structure without the damper experiences residual drift due to plastic deformations.

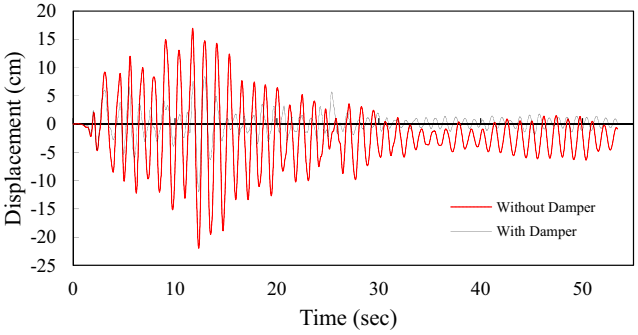

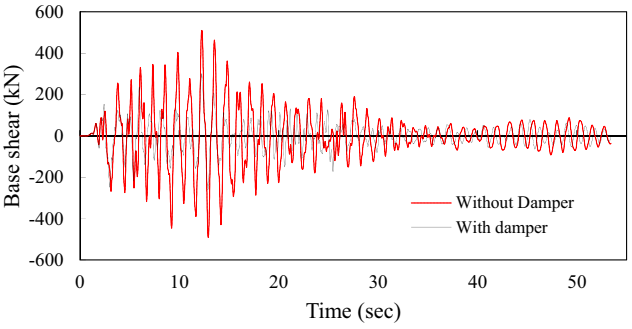

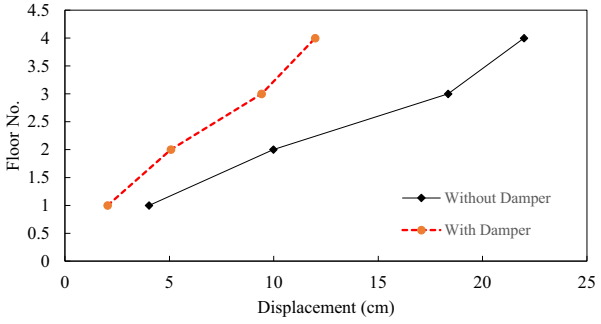

Fig. 23 – Effect of using one LRD per floor on the response of the 4-story steel frame under the Kobe 0.1 g earthquake.

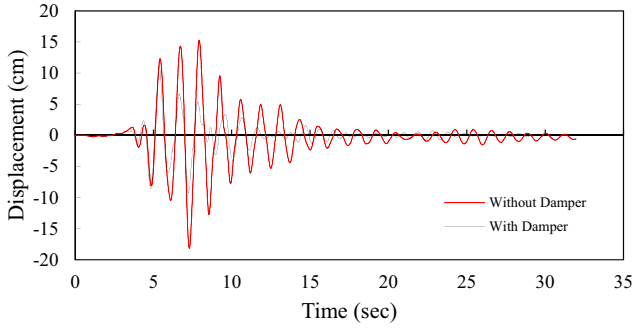

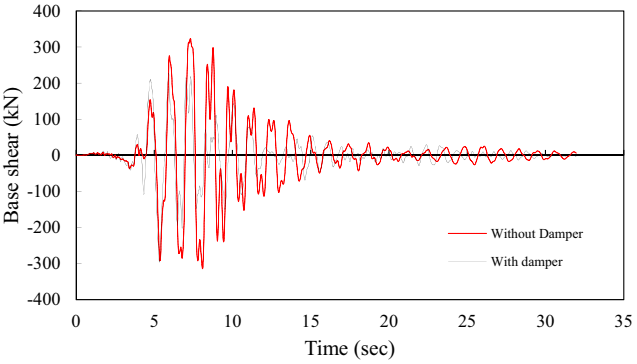

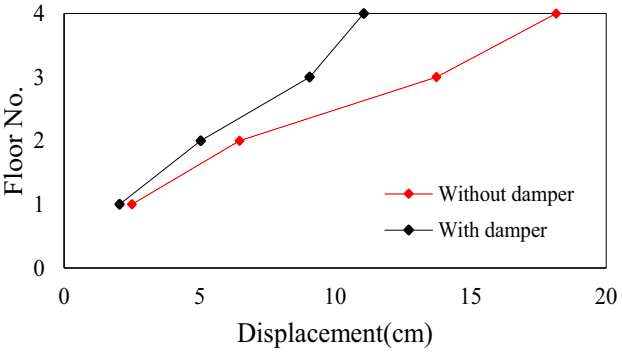

Fig. 24 – Effect of using one LRD per floor on the response of the 4-story steel frame under the Kobe 0.25 g earthquake.

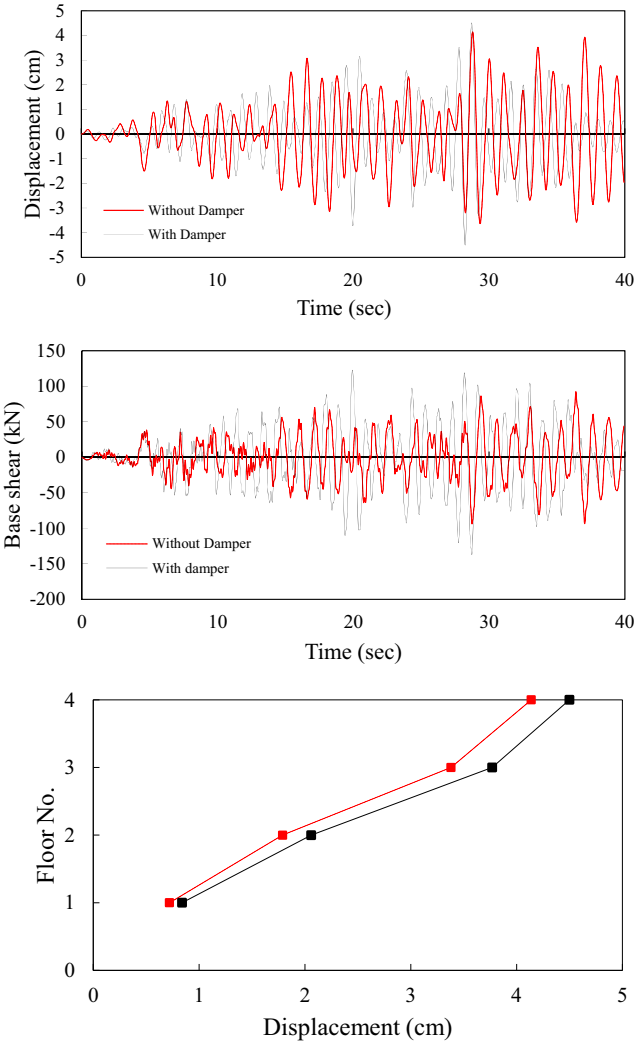

Fig. 25 – Effect of using one LRD per floor on the response of the 4-story steel frame under the Tabas 0.1 g earthquake.

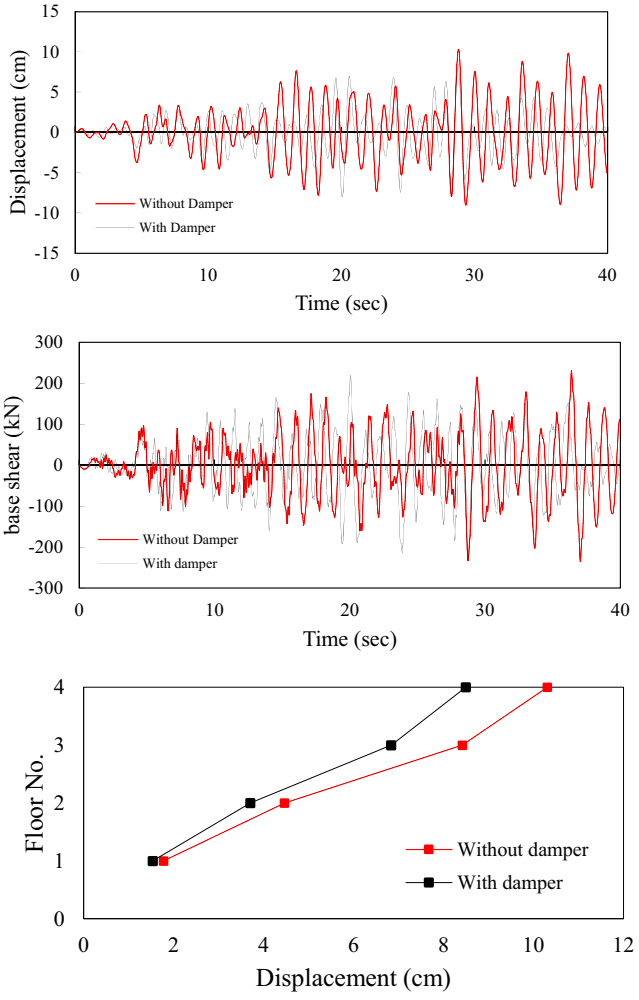

Fig. 26 – Effect of using one LRD per floor on the response of the 4-story steel frame under the Tabas 0.25 g earthquake.

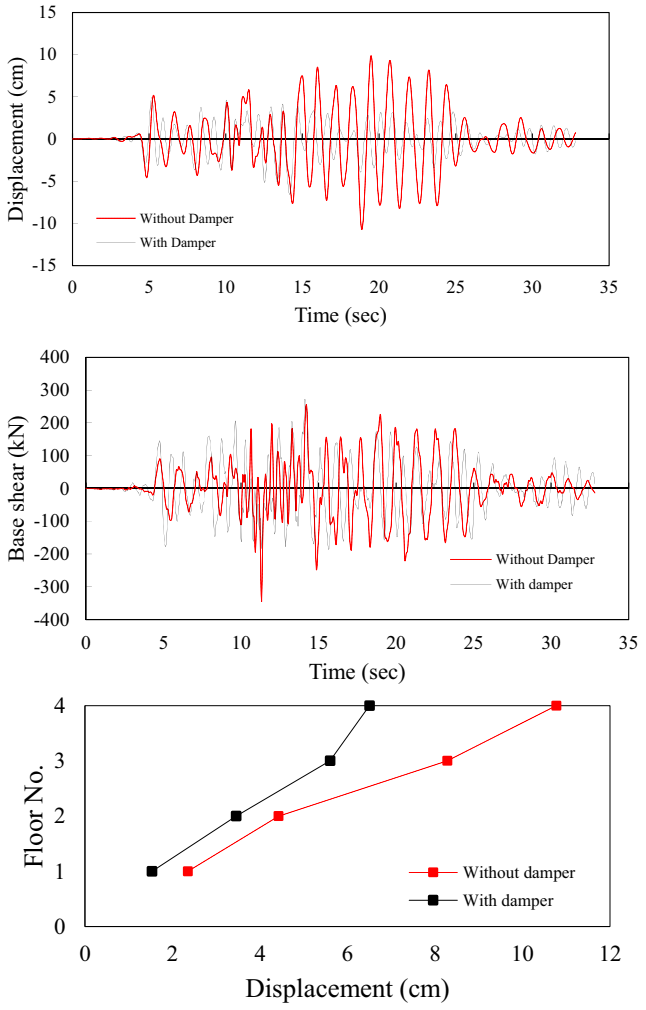

Fig. 27 – Effect of using one LRD per floor on the response of the 4-story steel frame under the Tabas 0.3 g earthquake.

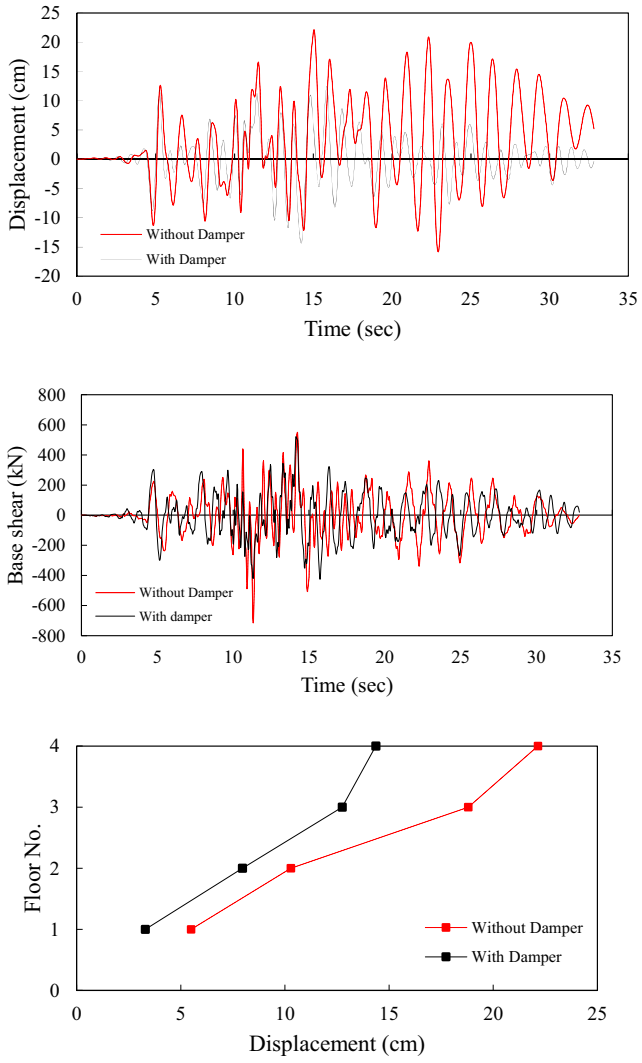

Fig. 28 – Effect of using one LRD per floor on the response of the 4-story steel frame under the Tabas 0.75 g earthquake.

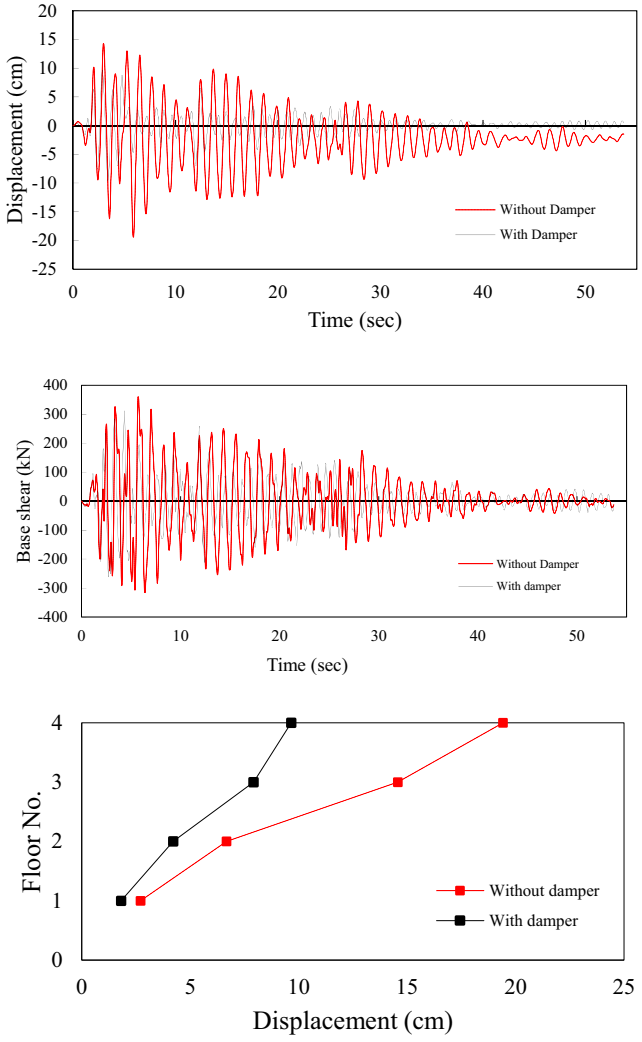

Fig. 29 – Effect of using one LRD per floor on the response of the 4-story steel frame under the Imperial Valley 0.3 g earthquake.

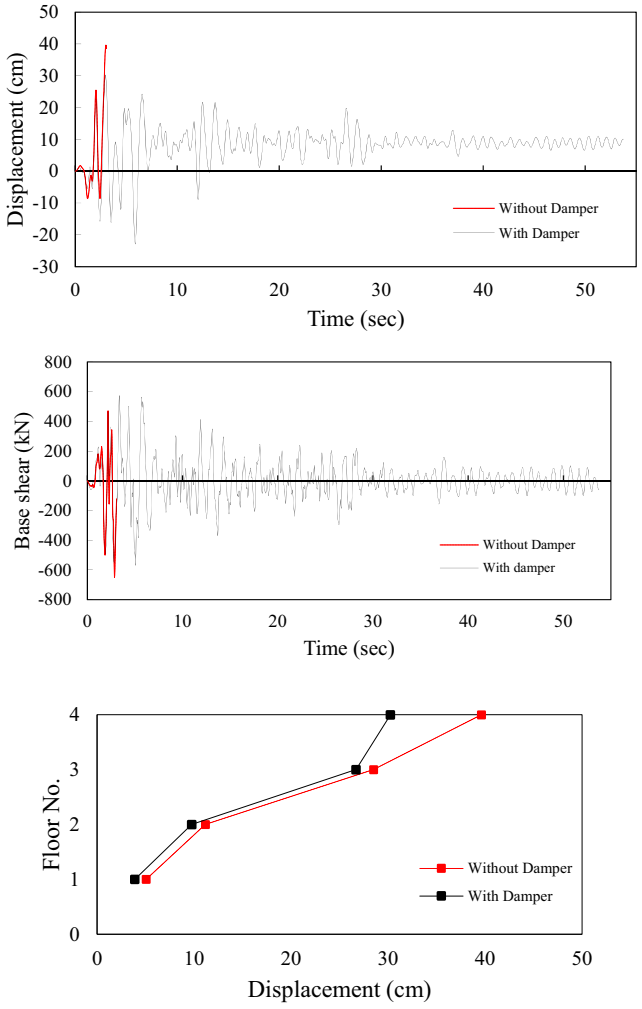

Fig. 30 – Effect of using one LRD per floor on the response of the 4-story steel frame under the Imperial Valley 0.75 g earthquake.

10. Conclusions

In this research, LRDs have been utilized in chevron bracing to protect structures against earthquake excitations. In this regard, experimental works and a detailed finite element model of the system were expanded. Finally, a four-story, three-bay steel frame equipped with the LRD was examined numerically under three scaled seismic excitations. The conclusions are as noted below:

1. According to the results of these analyses, the lead-rubber device can significantly improve the response of the frame, and the results indicates that the structure with the LRD remain elastic. In this configuration, the device is in a hand reaching position and can be surveyed or even replaced much easier than the other devices can.
2. The lead-rubber damper can reduce the story drifts and displacements. The average amount of the displacements in the 4-story steel frame under the El Centro, Kobe and Tabas earthquakes was decreased by 48%, 30% and 15%, respectively.
3. The LRD exhibits high reliability and proper functioning due to its simple producing and monitoring processes during manufacturing. Because the lead core is under hydrostatic pressure, the fatigue failure will not occur, and the damper will remain stable. Additionally, the construction cost is much lower than other dampers because there is no need for high technology manufacturing.

Acknowledgments

This research was supported by a grant (17CTAP-C129811-01) from Land Transport Technology Promotion Research Project Program funded by Ministry of Land, Infrastructure and Transport of Korean Government.

REFERENCES

[1] J.W. Hu, Response of seismically isolated steel frame buildings with sustainable lead-rubber bearing (LRB) isolator devices subjected to near-fault (NF) ground motions, Sustainability 7 (1) (2015) 111–137.
[2] J.W. Hu, Seismic analysis and parametric study of SDOF lead-rubber bearing (LRB) isolation systems with recentering shape memory alloy (SMA) bending bars, Journal of Mechanical Science and Technology 30 (7) (2016) 2987–2999.
[3] I. Mansouri, G. Ghodrati Amiri, J.W. Hu, M. Khoshkalam, S. Soori, S. Shahbazi, Seismic fragility estimates of LRB base isolated frames using performance-based design, Shock and Vibration 2017 (2017) 20.
[4] K. Shiba, S. Mase, Y. Yabe, K. Tamura, Active/passive vibration control systems for tall buildings, Smart Materials and Structures 7 (5) (1998) 588–598.
[5] T.T. Soong, G.T. Skinner, Experimental study of active structural control, Journal of Engineering Mechanics Division, ASCE 107 (6) (1981) 1057–1067.
[6] Y.L. Xu, J. Teng, Optimum design of active/passive control devices for tall buildings under earthquake excitation, Structural Design of Tall Buildings 11 (2) (2002) 109–127.
[7] K.C. Chang, T.T. Soong, M.L. Lai, E.J. Nielsen, Viscoelastic dampers as energy dissipation devices for seismic applications, Earthquake Spectra 9 (3) (1993) 371–387.
[8] D.K. Nims, P.J. Richter, R.E. Bachman, The use of the energy dissipating restraint for seismic hazard mitigation, Earthquake Spectra 9 (3) (1993) 467–489.
[9] A.G. Tarics, D. Way, J.M. Kelly, The Implementation of Base Isolation for the Foothill Communities Law and Justice Center, Report to the National Science Foundation, 1984.
[10] F. Naeim, J.M. Kelly, Design of Seismic Isolated Structures, John Wiley and Sons, New York, 1999.
[11] M.C. Constantinou, A.S. Whittaker, Y. Kalpakidis, D.M. Fenz, G.P. Warn, Performance of seismic isolation hardware under service and seismic loading, Technical report MCEER-07-0012, Buffalo, NY, 2007.
[12] I.V. Kalpakidis, M.C. Constantinou, Effects of heating and load history on the behavior of lead-rubber bearings, Technical report MCEER-08-0027, Buffalo, NY, 2008.
[13] H.S. Monir, K. Zeynali, A modified friction damper for diagonal bracing of structures, Journal of Constructional Steel Research 87 (2013) 17–30.
[14] C.J. Derham, J.M. Kelly, A.G. Thomas, Nonlinear natural rubber bearings for seismic isolation, Nuclear Engineering and Design 84 (3) (1985) 417–428.
[15] S.T. Jenq, H.-H. Chang, Y.-S. Lai, T.-Y. Tsai, High strain rate compression behavior for Sn–37Pb eutectic alloy, lead-free Sn–1Ag–0.5Cu and Sn–3Ag–0.5Cu alloys, Microelectronics Reliability 49 (3) (2009) 310–317.
[16] H.-C. Tsai, S.-J. Hsueh, Mechanical properties of isolation bearings identified by a viscoelastic model, International Journal of Solids and Structures 38 (1) (2001) 53–74.
[17] E.M. Arruda, M.C. Boyce, A three-dimensional constitutive model for the large stretch behavior of rubber elastic materials, Journal of the Mechanics and Physics of Solids 41 (2) (1993) 389–412.
[18] S. Kawabata, Y. Yamashita, H. Ooyama, S. Yoshida, Mechanism of carbon-black reinforcement of rubber vulcanizate, Rubber Chemistry and Technology 68 (2) (1995).
[19] R.W. Ogden, D.G. Roxburgh, A pseudo-elastic model for the Mullins effect in filled rubber, in: Proceedings of the Royal Society of London, 1988, 2861–2877.
[20] O.H. Yeoh, Some forms of the strain energy function for rubber, Rubber Chemistry and Technology 66 (5) (1993) 754–771.
[21] P. Raos, Modelling of elastic behaviour of rubber and its application in FEA, Plastics, Rubber and Composites Processing and Applications 19 (5) (1993) 293–303.
[22] J. Yoshida, M. Abe, Y. Fujino, Constitutive model of high-damping rubber materials, Journal of Engineering Mechanics 130 (2) (2004) 129–141.
[23] A.F.M.S. Amin, M.S. Alam, Y. Okui, An improved hyperelasticity relation in modeling viscoelasticity response of natural and high damping rubbers in compression: experiments, parameter identification and numerical verification, Mechanics of Materials 34 (2) (2002) 75–95.
[24] F. Zhu, H. Zhang, R. Guan, S. Liu, Effects of temperature and strain rate on mechanical property of $Sn_{96.5}Ag_3Cu_{0.5}$, Journal of Alloys and Compounds 438 (1–2) (2007) 100–105.